Tribology and Materials
Vol. 3, No. 4, 2024, pp. 150-162

ISSN 2812-9717
https://doi.org/10.46793/tribomat.2024.016

Surface texturing for tribomechanical performance optimisation of epoxy composites reinforced with chemically activated carbon

Leonard Maduabuchi AKUWUEKE, Chinwuba Victor OSSIA*, Harold Ugochukwu NWOSU

Faculty of Engineering, University of Port Harcourt, Port Harcourt, Nigeria
*Corresponding author: chinwuba.ossia@uniport.edu.ng

Keywords

surface texturing
tribomechanical properties
agro-waste
activated carbon
composites
Box-Behnken design

History

Received: 12-08-2024
Revised: 19-11-2024
Accepted: 26-11-2024

Abstract

The effects of surface texturing on the tribomechanical properties of epoxy composites reinforced with chemically activated carbon were studied. Activated carbon produced from palm kernel (PKSAC) and coconut shells (CSAC) were composed in three concentrations (X_{CSAC}): 100 vol. % CSAC + 0 vol. % PKSAC, 50 vol. % CSAC + 50 vol. % PKSAC and 0 vol. % CSAC + 100 vol. % PKSAC, three particle sizes (X_{PS}): 60, 105 and 150 µm, three reinforcement amounts (X_{RW}): 4, 6 and 8 wt. %, and used to fabricate cylindrical discs of Ø 50 × 6 mm height with four surface texture geometries. The epoxy/activated carbon composites were experimentally evaluated for tribomechanical performance using Box-Behnken design. Multivariate second-order polynomial models approximated the influence of X_{CSAC}, X_{PS} and X_{RW} on the tribomechanical properties. The aim was to use the property response to determine the effect of texturing on the tribomechanical properties of composites for automobile applications. The maximum tensile strength value was the highest for the untextured surface, followed in descending order by circular, triangular and rectangular surface texture. The maximum compressive strength value was the highest for the untextured surfaces, followed in descending order by triangular, circular and rectangular surface texture. The maximum wear rate value was the highest for the untextured surfaces, followed in descending order by rectangular, circular and triangular surface texture, while the maximum coefficient of friction value was the highest for the circular surface texture, followed in descending order by triangular and rectangular surface texture and untextured surfaces. Texturing surfaces were found to reduce the composites' mechanical properties while decreasing the wear rate and increasing the coefficient of friction.

1. Introduction

The surface characteristics of any object can be described as its texture. The degree of surface texture is generally defined concerning its form, roughness and waviness [1]. The effect of surface texture when used in different friction applications has not been well established. With different applications in mind, high friction can be required for specific purposes such as brakes, vehicle tyres, clutches and other transmissions. However, friction reduction can be desirable in some applications. Hence, texturing surface is one of the techniques that can be used to control friction at interfaces. New composite materials with exceptional mechanical properties have been developed and utilised for various engineering applications. Over the past ten years, polymer composites reinforced with natural fibres have found applications in sporting products, automotive parts, medical devices, sea vehicles and the aerospace industry, due to their minimum cost, elevated specific strength, lesser weight, higher resistance to wear and corrosion, etc [2].

The mechanical characteristics of polyester composites reinforced with natural hybrid fibres made of 108 cotton samples collected in fibre form from a spinning mill in Kenya were studied according to fibres length and weight percentage [3]. It was concluded from the prediction models that the most effective fibre properties on yarn strength were breaking elongation, fibre length, micronaire value and fibre trash content. The mean micronaire value was reported as 2.74, while the mean fibre trash content was 7.99 % [3]. Micronaire is a measure of the air permeability of compressed cotton fibres. It is often used as an indication of fibre fineness and maturity. Fibre fineness and maturity are critical for fibre processing, as well as fibre quality [3]. Fibre trash content in cotton refers to non-fibre particles such as leaf, seed coat, bark, grass, dust and other foreign matters. Trash content in cotton is highly considered in the present cotton grading system because the presence of trash degrades yarn evenness, yarn strength and fabric appearance and causes problems in textile processing [4].

The surface roughness of the drilled polymer composites reinforced with glass fibre has been predicted using fuzzy logic rule-based modelling and ANOVA [5]. The experimental values showed good agreement when compared with the model results. From the analysis, it is clear that the feed rate with 69.21 % influence is the main parameter that significantly affects the mean average surface roughness. The drill diameter with 23.65 % and spindle speed with 1.75 % influences also affect the surface roughness. The interaction between the parameters does not pose much influence. Among the three interactions considered, only the interaction between the feed rate and drill diameter has a small effect on the surface roughness.

Based on the literature review, friction can be improved by using surface texturing. In the study conducted by Hammerström and Jacobson [6], it was concluded that pyramid-textured surfaces lubricated with polyalfaolefin (PAO) showed a high coefficient of friction. Bio-inspired polymeric patterns fabricated on SU-8 polymer film showed excellent wear resistance and low frictional properties [7]. The research performed by Dumitru et al. [8] showed that, due to the presence of micro textures on steel discs, the wear resistance of the samples improved eight times more than that of the untextured specimens. The benefits of surface texture in tribology can be enhanced by adjusting the different texture parameters like density, orientation, size, pattern and depth. Positive (protuberances) asperities and negative (recesses) valleys can be developed on surfaces. Such protuberances on surfaces can result in real contact area and friction reduction. Different surface patterns can be used to improve tribological behaviours in unlubricated conditions by adjusting the contact conditions. Researchers have reported that several surface textures like micro dimples or grooves can significantly reduce friction [9,10].

Carbon fibre-reinforced epoxy composites present engineering materials with relatively higher mechanical properties required in the aeronautical industry [11,12]. Carbon fibres are extensively used where higher strength and wear resistance polymer matrix composites are required [13]. According to studies, it has been found that the addition of nanoparticles into the matrix can enhance the tribological and mechanical properties of the composites [14,15]. The abrasive wear behaviour of epoxy reinforced with carbon, glass and aramid fabrics was investigated by Friedrich [16]. The coefficient of friction and wear of carbon fibre-reinforced epoxy composites was found to reduce with the addition of spherical TiO_2 nanoparticles [17]. The short carbon fibres were found to be protected from severe wear due to the rolling effect of TiO_2. Chang and Zhang [18] investigated the filler effect on wear resistance of epoxy filled by nano-size TiO_2, graphite, polytetrafluoroethylene and short carbon fibre. It was concluded that nano-size TiO_2 and short carbon fibre showed the best wear resistant composition. A substantially lower coefficient of friction was obtained for epoxy composites reinforced by unidirectional carbon fibres when fibres were parallel to the sliding direction [19]. High wear resistance was noticed in composites reinforced by carbon fibres [20]. This is favourable for composites used as antifriction bearings and guideways. The epoxy/unidirectional woven carbon fibre composites with fibres parallel to the sliding direction had a lower coefficient of friction and higher abrasive wear resistance [21].

Response surface methodology (RSM) is an empirical modelling technique used for developing, improving and optimising the process to evaluate the relationship between a set of controlled experimental factors and obtained results [22]. Three major steps are involved in the optimisation process: performing the experiments statistically designed, estimating the coefficients in a mathematical model and predicting the response and checking the suitability of the model. The factors are optimised by changing one factor at a time and keeping other variables constant in the conventional approach. RSM is capable of simultaneously determining the individual and interactive effects of many factors [23]. Optimisation using RSM has been widely applied in the development of natural cellulosic fibre-reinforced composites. In the fabrication of wool fibre-reinforced polypropylene composites, the optimum mechanical properties were obtained at 176 °C, for 7 minutes at 3.5 MPa in a compression moulding machine [24]. The tensile strength of the palmyra fibre-reinforced composite was greatly influenced by the alkali treatment time, fibre length and fibre volume fraction [25]. The fibre content greatly influenced the tensile and flexural properties of the flax fibre-reinforced polyethylene biocomposites compared to injection moulding temperature and pressure. The tensile strength and flexural strength of the composites increased with an increase in fibre content. The composites processed below 190 °C produced better mechanical properties [26]. The compression moulding process parameters for the development of silk fibre-reinforced polypropylene composites were optimised using the Box-Behnken experimental design. The trimmed silk fibres from shuttleless loom silk selvedge waste were used as reinforcement in the polypropylene fibre matrix. The temperature (165 – 185 °C), time (7 – 15 minutes) and pressure (3.5 – 4.5 MPa) of compression moulding were optimised concerning the mechanical properties of the silk fibre-reinforced polypropylene composite. The optimum parameters for better mechanical properties were found to be a temperature of 180 °C, time of 7 minutes and pressure of 3.5 MPa. The optimised level of parameters showed a good response to the predicted model [27].

The effect of process parameters on the mechanical properties of the Agave sisalana Variegata fibre-reinforced vinyl ester composites was studied using Box-Behnken design (BBD) [28]. The fibre length of 13 mm, fibre content of 35.19 wt. % and fibre diameter of 0.24 mm were selected as the optimal values of fabrication process parameters using the response surface graph and models. The results show that the tensile and flexural strength can be predicted by the developed models with more than 98.54 % of the variation in the tensile strength and 99.24 % of the variation in the flexural strength. Finally, it was proved that the BBD of response surface methodology could efficiently be applied to the modelling and optimisation of the mechanical properties of natural fibre-reinforced polymer composites [28].

To have a better understanding and to determine the effects of surface texturing on the tribomechanical properties of the composites reinforced with chemically activated carbon, the experimental tests were performed based on BBD. Using these sets of data obtained with experimental tests, responses were then developed to show the effect of surface texturing on the tribomechanical properties of the composites. This study derived its novelty by investigating the effects of negative surface texturing on the tribological and mechanical properties of the newly developed epoxy composites reinforced with chemically activated carbon for brake pad application. This study showed its novelty by investigating the effects of negative surface texturing on the tribological and mechanical properties of the newly developed epoxy composites reinforced with chemically activated carbon for brake pad application.

2. Materials and methods

2.1 Production of activated carbon

The activated carbon was produced using palm kernel shells and coconut shells as precursors. The produced activated carbons were designated as palm kernel shell activated carbon (PKSAC) and coconut shell activated carbon (CSAC). Materials and equipment used include $CaCl_2$, aluminium pot, distilled water and ramming mass (castable). The methodology employed in the production of the activated carbons is reported elsewhere [29]. To produce the chemically activated carbon, the precursor was first pyrolysed in a temperature range of 260 – 265 °C. The charred materials were then washed in tap water and spread in the open for sun drying for 4 days. The charred materials were then ball-milled to reduce the granule size. To produce the activated carbon after pyrolysis, $CaCl_2$ was mixed with distilled water in a ratio of 1:3 (100 g of $CaCl_2$ was mixed with 300 ml of distilled water) in a volumetric flask and stirred to form a solution. The biochar granules were then mixed with the $CaCl_2$ solution in a ratio of 2:1 (300 g of biochar granules was mixed with 150 ml of solution). The mixture was stirred continuously until a paste-like material was formed. The paste-like material was covered and left for 24 hours. Water was drained from the samples as much as possible and the samples were transferred into an aluminium pot with a lid and was heated for 3 hours to activate. Samples with surface texture were fabricated after the production of the activated carbon.

2.2 Models of surface textures

The drafting of the surface textures was done using AutoCAD 2016 software. A circular (Ø 4 mm) dimple with a depth of 4 mm, a rectangular (5 × 2.5 mm) dimple with a depth of 4 mm and an equilateral triangular (5 mm) dimple with a depth of 3.5 mm were used in the drafting. The models of circular, rectangular and triangular textured samples are shown in Figure 1.

2.3 Fabrication of surface textured composites

The fabrication of the surface-textured epoxy/activated carbon composite discs for experimentation was performed using lost-wax moulding and casting, which uses beeswax. The activated carbon types (100 vol. % CSAC + 0 vol. % PKSAC, 50 vol. % CSAC + 50 vol. % PKSAC and 0 vol. % CSAC + 100 vol. % PKSAC) were prepared into dimpled surfaces using epoxy resin, bronze mould, cassava starch, caustic soda, carving knife and cardboard pattern. A 50 g of beeswax was melted in 0.25 litres of water in a cylindrical container of Ø 50 mm and 100 mm depth, heated to 100 °C and cooled to ambient temperature. The solidified beeswax was then removed and placed on a flat substrate. The cardboard profile pattern was placed over the beeswax and the various individual dimple patterns were carved out. The profile pattern paper with Ø 50 mm was placed inside the bronze mould. The previously carved out individual beeswax patterns were fixed on the individual spaces provided on the paper and talc was then applied on the mould walls. A 10 ml of epoxy resin and hardener were mixed and poured into the mould and left for 24 hours to cure, then removed. This acts as the pattern for producing the textured surface of the epoxy/activated carbon composites. Starch, water and liquid caustic soda were mixed to a consistent thick slurry. About 20 ml of the thick slurry was poured into the bronze mould and then the earlier prepared epoxy pattern was placed over it, with face down. A pressure of 10 N was applied to the epoxy pattern and allowed to cure under moderate heat. The epoxy pattern was then removed, leaving the slurry pattern inside the bronze mould.

The weight ratios were calculated and used to mix the reinforcement with epoxy matrix (Epochem 105 epoxy resin and Epochem 205 epoxy catalyst) and poured into the mould whose internal side wall has been rubbed with talc for easier product removal. The samples were allowed for 24 hours to cure. After that, the samples were immersed in water heated at 70 °C for about 2 minutes, and then the mould was turned over and the sides were gently tapped for the casting to drop. Then the surface is ground on a polishing machine. The process was repeated to produce the various texture geometries (circular, rectangular and triangular textures) on the surfaces of the composites fabricated with different reinforcement weight percentages and particle sizes and different PKSAC/CSAC concentrations. The same beeswax was reused for subsequent patterns and castings.

Figure 2a shows the mould used to produce the untextured (plane) epoxy/activated carbon composite disc samples before casting. Figure 2b shows the texture pattern preparation before casting, while Figure 2c shows textured moulds having circular, rectangular and triangular geometries before casting. Representative samples of the produced textured epoxy/activated carbon composite discs are shown in Figure 3. As-cast average dimensions of all discs were 50.6 mm in diameter and 6.0 mm in thickness. The as-cast specifications dimensions of textured surfaces are shown in Table 1.

Table 1. As-cast specifications of textured surface

Dimple			
shape	cross-section dimensions, mm	average depth, mm	number
circular	Ø 3.8	3.5	42
rectangular	4.3 × 3.0	4	38
triangular	4.82 × 4.82 × 4.82	3.5	39

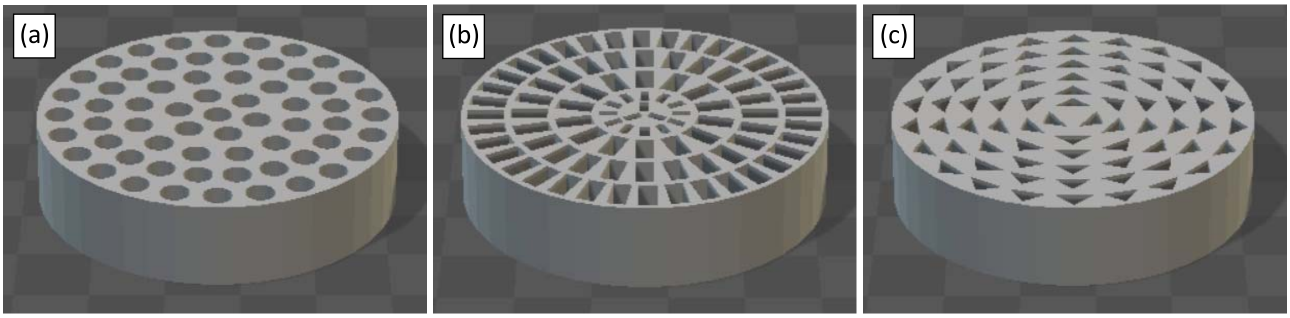

Figure 1. 3D solid model of surface texture: (a) circular, (b) rectangular and (c) triangular

Figure 2. Moulds preparation: (a) moulds with thick slurry applied, (b) texture pattern positioned in mould and (c) beeswax dimples positioned in moulds

Figure 3. Samples with textured surface: (a) circular, (b) triangular and (c) rectangular

2.4 Mechanical properties of surface textured samples

The tensile strength of the surface textured samples was obtained by a tensile test conducted on the universal testing machine Ametek EZ250, following the ASTM D638 standard.

Compressive tests were performed following the ASTM D3410 standard using the universal testing machine Ametek EZ250.

To determine the flexural strength of the surface textured samples, a three-point flexural test was conducted on the universal testing machine Ametek EZ250. The procedure followed the ASTM D790 standard, with a crosshead speed of 2 mm/min and a span length of 30.22 mm.

To obtain the average Shore D hardness value of the surface textured samples, tests were conducted at three different points on the sample, each between two dimples, following a 3^3 factor Box-Behnken design of experiment using an analogue Shore D scale durometer SHD0002 (CV Instruments). The sample preparation and procedure followed the ASTM D2240 standard.

2.5 Tribological properties of surface textured samples

The friction and wear performance tests of the surface textured disc samples were performed using a ball-on-disc tribometer TRB^3 (Anton Paar) under the conditions specified in Table 2. Samples were prepared following the ASTM G99 standard. The wear rate was calculated as mass loss per sliding distance [30].

Table 2. Tribological test conditions

Sliding condition	Dry
Normal load, N	10
Sliding speed, cm/s	10
Sliding distance, m	96
Wear track diameter, mm	10
Air humidity, %	55
Ambient air temperature, °C	27 – 29

The properties of the stainless steel test ball, with Ø 6 mm, used as a counter-body were: hardness of 800 VHN, tensile strength of 1500 MPa, compressive strength of 1000 MPa and thermal conductivity of 50 W/mK.

2.6 Testing design for surface textured samples

The optimisation of the tribomechanical properties concerning the input variables was performed using Box-Behnken design (BBD). A total of 15 experimental runs based on 3^3 BBD were used. The main aim of this technique is to optimise the response influenced by various process parameters. It also quantifies the relationship between the controllable input process parameters and the obtained response [31]. Table 3 shows the process parameters (factors) data while Table 4 shows the BBD input parameters combination for the experimental runs. These factors were determined based on a preliminary investigation. The influence of the 3 factors: activated carbon type X_{CSAC}, reinforcement amount X_{RW} and reinforcement particle size X_{PS} on the tribological and mechanical properties was approximated by the following second-order model equation [32].

$$Y = \beta_o + \sum_{i=1}^{3} \beta_i X_i + \sum_{i \neq j=1}^{3} \beta_{ij} X_i X_j + \sum_{k=1}^{3} \beta_{kk} X_k^2 + e, \quad (1)$$

where Y is the predicted tribomechanical property outcome for the epoxy/activated carbon composites with an untextured/textured surface, β_o is the model constant, β_i is the linear (main) coefficient, β_{kk} is the quadratic coefficient, β_{ij} is the interaction coefficient, X_i, X_j and X_k are the coded or normalised independent variables and e is the experimental error.

Table 3. Parameters, factors and their levels

Parameter (coded factor)	Level		
	Low	Medium	High
Reinforcement particle size X_{PS}, µm (X_1)	60 (−1)	105 (0)	150 (+1)
Reinforcement amount X_{RW}, wt. % (X_2)	4 (−1)	6 (0)	8 (+1)
CSAC concentration X_{CSAC}, vol. % (X_3)	0 (−1)	50 (0)	100 (+1)

Table 4. Input parameters for each experimental run

Run	Reinforcement particle size, µm	Reinforcement amount, wt. %	CSAC concentration, vol. %
1	60	4	50
2	150	4	50
3	60	8	50
4	150	8	50
5	60	6	100
6	150	6	100
7	60	6	0
8	150	6	0
9	105	4	100
10	105	8	100
11	105	4	0
12	105	8	0
13	105	6	50
14	105	6	50
15	105	6	50

The equations relating the independent variables with the normalised factors are given in Equations (2), (3) and (4) for reinforcement particle size factor X_1, reinforcement amount factor X_2 and activated carbon type factor X_3 as a function of reinforcement particle size X_{PS}, reinforcement amount X_{RW} and coconut shell activated carbon (CSAC) concentration X_{CSAC}, respectively.

$$X_1 = \frac{X_{PS} - 105}{45}, \quad (2)$$

$$X_2 = \frac{X_{RW} - 6}{2}, \quad (3)$$

$$X_3 = \frac{X_{CSAC} - 50}{50}. \quad (4)$$

3. Results and discussion

Tables 5 to 8 show the results obtained from the experimental runs for untextured samples and circular, rectangular and triangular surface textured samples, respectively. The average results of the tribomechanical properties of the various surface textures from the experimental runs are also presented for comparison.

3.1 Tensile strength

It was noticed that tensile strength was reduced with texturing. The untextured surface samples showed higher tensile strength than the textured surface samples. The tensile strength predicted values, for different surface texture conditions were in the following order: untextured (16.16 – 22.63 MPa), circular texture (8.36 – 15.94 MPa), triangular texture (5.26 – 13.48 MPa) and rectangular texture (6.66 – 12.07 MPa). This represented a reduction of 48 and 30 % for a minimum and maximum value of circular dimples, 67 and 40 % for a minimum and maximum value of triangular dimples and 59 and 47 % for a minimum and maximum value of rectangular dimples. All percentages are with respect to the untextured surfaces. The sharp fillet edges on the rectangular dimples played a significant role in determining the peak stresses, hence reducing tensile strength.

Figure 4 shows the tensile strength variation of untextured and circular rectangular and triangular textured surfaces. Comparing maximum values of the four textured geometries, the order was as follows: untextured (22.63 MPa), circular texture (15.94 MPa), triangular texture (13.48 MPa) and rectangular texture (12.07 MPa). The tensile strength response of rectangular textured surface and untextured surface were concave-shaped, unlike the convex-shaped response of circular and triangular textured surfaces. As the tensile force is applied to the material, it tends to dislodge the microstructure of the material increasing stress concentration at the edges of the texture thereby reducing the tensile strength of the textured surfaces compared with the untextured surface. The peak stress occurred

Table 5. Results obtained from the experimental runs for untextured surface

Run	Composite output (tribomechanical) property					
	Tensile strength, MPa	Compressive strength, MPa	Flexural strength, MPa	Hardness (Shore D)	Wear rate × 10^{-6}, g/m	Coefficient of friction
1	19.12	38.53	28.21	75.5	39.58	0.08
2	24.85	30.08	41.63	72	13.54	0.11
3	10.64	40.34	32.43	77	18.75	0.25
4	12.86	35.80	32.27	79	12.50	0.24
5	17.19	39.08	35.33	80	9.38	0.11
6	21.66	26.94	40.14	77	2.08	0.01
7	20.15	27.22	44.38	69	26.04	0.23
8	18.82	31.37	43.00	81	10.42	0.09
9	20.64	43.20	32.36	76	6.25	0.10
10	15.45	36.99	31.26	73	16.67	0.14
11	10.37	29.16	20.58	65	19.79	0.39
12	22.87	41.44	36.50	74.5	14.58	0.09
13	16.60	27.86	43.58	60	25.00	0.13
14	16.60	27.86	43.58	60	30.21	0.13
15	16.60	27.86	43.58	60	33.33	0.10
Average value	17.63	33.58	36.59	71.93	18.54	0.15

Table 6. Results obtained from the experimental runs for circular surface texture

Run	Composite output (tribomechanical) property					
	Tensile strength, MPa	Compressive strength, MPa	Flexural strength, MPa	Hardness (Shore D)	Wear rate × 10^{-6}, g/m	Coefficient of friction
1	10.43	19.60	27.19	68	42.71	0.10
2	14.90	25.46	32.96	68	26.04	0.10
3	11.62	26.07	36.33	67	21.88	0.13
4	11.23	17.48	23.43	66	19.79	0.35
5	8.93	19.94	25.57	69	6.25	0.30
6	10.80	20.90	25.84	68	34.38	0.17
7	18.14	24.08	33.30	71	8.33	0.35
8	9.28	23.23	34.84	69	13.54	0.44
9	13.61	24.32	33.92	72	11.46	0.09
10	8.61	18.39	23.19	71	10.42	0.09
11	11.95	23.73	27.11	70	17.71	0.10
12	11.42	23.02	27.23	72	20.83	0.19
13	13.32	23.89	35.02	66	27.08	0.02
14	13.32	23.89	35.02	66	18.75	0.11
15	13.32	23.89	35.02	66	17.71	0.19
Average value	12.06	22.53	30.40	68.60	19.79	0.18

Table 7. Results obtained from the experimental runs for rectangular surface texture

Run	Composite output (tribomechanical) property					
	Tensile strength, MPa	Compressive strength, MPa	Flexural strength, MPa	Hardness (Shore D)	Wear rate × 10^{-6}, g/m	Coefficient of friction
1	11.28	23.41	35.22	74	50.00	0.34
2	11.57	19.66	41.27	68	15.63	0.17
3	8.77	19.14	50.48	69	29.17	0.30
4	12.47	20.86	41.90	70	5.21	0.14
5	4.69	21.34	38.42	69	3.13	0.22
6	10.31	22.28	27.91	71	28.13	0.06
7	9.21	14.50	27.84	67	20.83	0.12
8	10.51	19.62	71.28	65	32.29	0.18
9	17.95	22.98	33.64	73	21.88	0.15
10	12.49	24.74	48.14	66	9.38	0.14
11	10.87	14.22	33.92	69	17.71	0.15
12	11.50	14.20	41.87	71	19.79	0.27
13	11.19	23.15	39.70	71	27.08	0.12
14	11.19	23.15	39.70	71	25.00	0.16
15	11.19	23.15	39.70	71	23.96	0.23
Average value	11.01	20.43	40.73	69.67	21.95	0.18

Table 8. Results obtained from the experimental runs for triangular surface texture

Run	Composite output (tribomechanical) property					
	Tensile strength, MPa	Compressive strength, MPa	Flexural strength, MPa	Hardness (Shore D)	Wear rate × 10^{-6}, g/m	Coefficient of friction
1	7.65	22.18	17.43	70	47.92	0.05
2	13.33	24.83	32.49	72	10.42	0.05
3	6.59	20.29	14.84	69	26.04	0.15
4	12.68	27.72	29.87	69	26.04	0.35
5	13.01	24.65	26.47	70	12.5	0.25
6	11.38	23.33	23.85	67	23.96	0.19
7	11.67	26.96	35.97	69	10.04	0.35
8	7.26	31.40	16.28	66	23.96	0.11
9	12.44	26.62	30.85	72	13.54	0.30
10	11.83	27.26	17.80	70	16.67	0.30
11	8.55	21.98	23.43	66	25.00	0.14
12	11.31	28.26	38.15	71	28.13	0.16
13	5.41	21.33	14.27	68	23.96	0.26
14	5.41	21.33	14.27	68	16.67	0.23
15	5.41	21.33	14.27	68	21.88	0.16
Average value	9.60	24.63	23.35	69.00	21.78	0.20

at the periphery of the triangular dimples having sharp fillet edges, which was consistent with the finding of Khemchandani et al. [33].

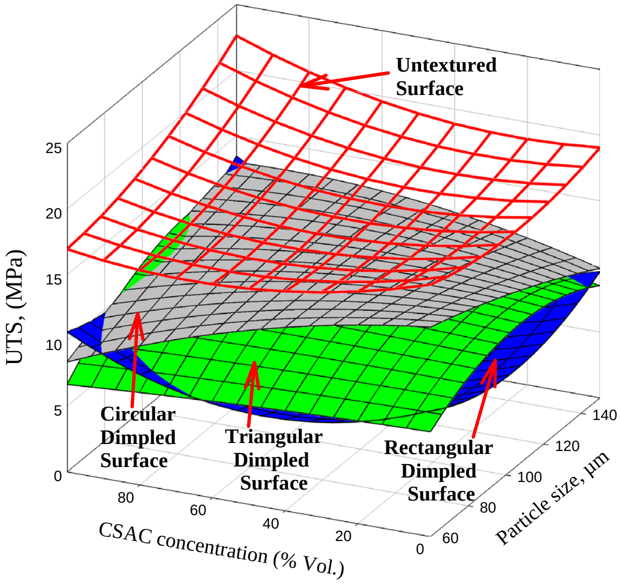

Figure 4. Tensile strength (UTS) variation obtained by the BBD for untextured and circular, rectangular and triangular textured surfaces

3.2 Compressive strength

It was noticed that compressive strength predicted values were reduced with sample texturing in the following order: untextured (25.74 – 39.97 MPa), circular texture (20.60 – 24.54 MPa), rectangular texture (14.29 – 24.34 MPa) and triangular texture (20.89 – 30.52 MPa). This represented a reduction of 20 and 39 % for a minimum and maximum value of circular dimples, 45 and 39 % for a minimum and maximum value of rectangular dimples and 19 and 24 % for a minimum and maximum value of triangular dimples. All percentages are with respect to the untextured surfaces.

Figure 5 shows that the maximum compressive strength responses of untextured and textured surfaces were in the following order: untextured (39.97 MPa), triangular texture (30.52 MPa), circular texture (24.54 MPa) and rectangular texture (24.34 MPa). During compressive loading, failure was noticed at the dimples sidewalls as compressive crack initiated at dimple tips. As the compressive force is applied to the material, it tends to dislodge the microstructure of the material increasing stress concentration at the edges of the textures thereby reducing the compressive strength of the textured surfaces compared with the untextured surface. Compared with the untextured surface, the existence of dimples further enhanced stress distribution between the two dimples. High-compressive stress concentrates at dimple side edges. This is consistent with the findings of other researchers [33,34].

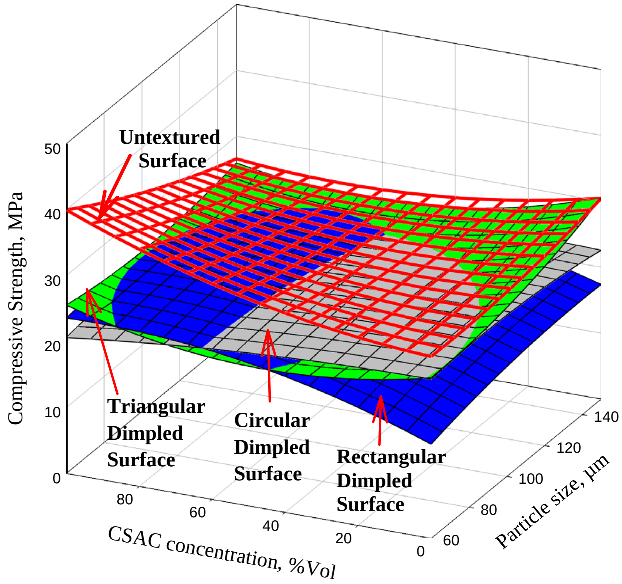

Figure 5. Compressive strength variation obtained by the BBD for untextured and circular, rectangular and triangular textured surfaces

3.3 Flexural strength

It was noticed that flexural strength was reduced with texturing. The untextured surface samples showed higher flexural strength than the textured samples in the following order: untextured (36.41 – 46.01 MPa), circular texture (27.16 – 35.28 MPa), rectangular texture (27.43 – 62.00 MPa) and triangular texture (13.99 – 30.80 MPa). This represented a reduction of 25 and 23 % for a minimum and maximum value of circular dimples, 25 % for a minimum value of rectangular dimples and 62 and 33 % for a minimum and maximum value of triangular dimples. The 26 % increase for a maximum value of rectangular dimples instead of a reduction was an isolated case. All percentages are with respect to the untextured surfaces. It was noticed that this increase occurred at 0 vol. % CSAC and a particle size of 150 µm.

From Figure 6, it was noticed that flexural strength responses of rectangular textured surfaces lie below the untextured surface, with these surfaces intercepting within the particle size range of 80 – 90 µm and CSAC range of 80 – 100 vol. %, and also within the particle size range of 100 – 120 µm and CSAC range of 0 – 40 vol. %. In this case, flexural strength for a rectangular textured surfaces was in the range of 27.43 – 45.85 MPa, which is lower than the values for an untextured surface.

The flexural stress interaction between dimples was a major reason for crack initiation and propagation. Compared with the untextured surface, the existence of dimples enhanced the stress between the dimples and high-flexural stress concentrated at dimple side edges, which was consistent with the findings of other researchers [33,34].

Comparing the four different surface textures it can be concluded that rectangular textured surface generally lay below the untextured surface, while the triangular textured surface lay below the rectangular textured surface. Within the range of rectangular textured and untextured surface intercepting, the flexural strength values were in the following order: untextured (46.01 MPa), rectangular texture (45.85 MPa), circular texture (35.28 MPa) and triangular texture (30.80 MPa). However, comparing the textured samples shown in Figure 6, the maximum flexural strength values were in the following order: rectangular texture (62.00 MPa), circular texture (35.28 MPa) and triangular texture (30.80 MPa).

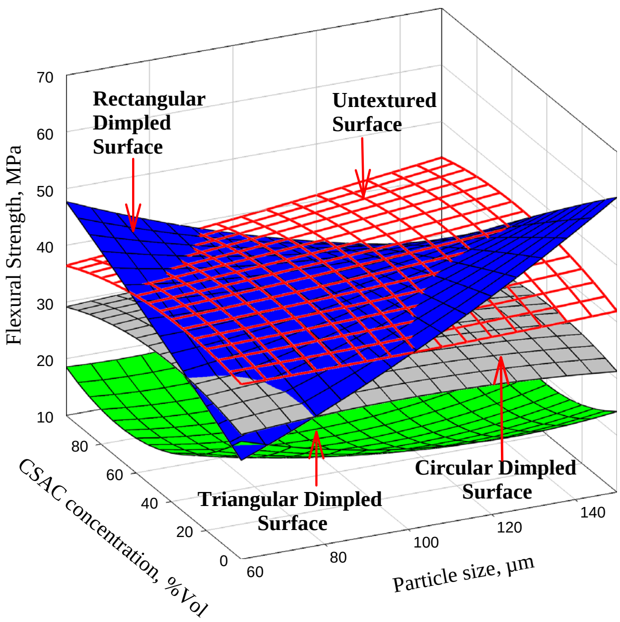

Figure 6. Flexural strength variation obtained by the BBD for untextured and circular, rectangular and triangular textured surfaces

3.4 Hardness

It was noticed from Figure 7 that samples with untextured surfaces had higher predicted values of hardness than samples with textured surfaces, with values in the following order: untextured (59.78 – 81.63), triangular texture (65.27 – 71.74), rectangular texture (65.50 – 71.14) and circular texture (65.14 – 70.25). This represents a reduction of maximum hardness of 12 % for triangular dimples, 13 % for rectangular dimples and 14 % for circular dimples. All percentages are with respect to the untextured surfaces.

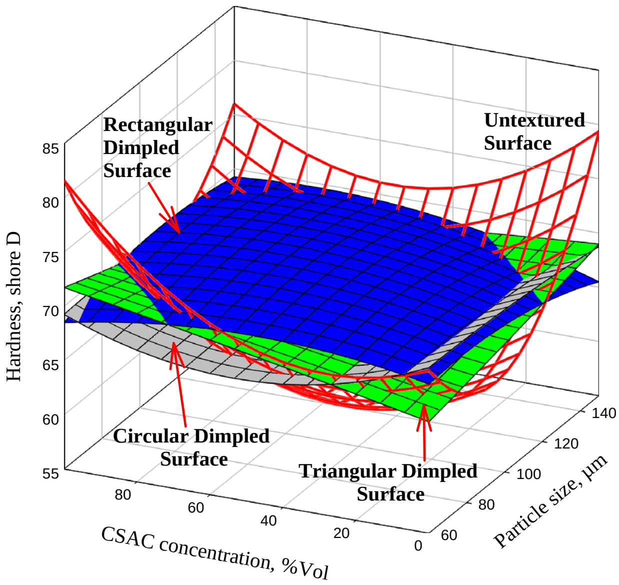

Figure 7. Hardness variation obtained by the BBD for untextured and circular, rectangular and triangular textured surfaces

As the indentor penetrates the sample, the force impacted on the material tends to dislodge the material's microstructure, causing a lateral movement of the matrix and reinforcement across the dimples. This enhances the stress on the edges of the textures, thereby reducing the hardness of the textured surfaces compared with the untextured surface. Comparing the hardness response of untextured surface with that of textured surfaces, the maximum hardness values were in the following order: untextured (81.63), triangular texture (71.74), rectangular texture (71.14) and circular texture (70.25). During the application of load to samples, inter-dimple stress was evident as samples were weakened due to non-resistance to lateral and vertical microstructure movement resulting in hardness reduction.

3.5 Wear rate

From Figure 8, the predicted values of wear rate obtained for each surface texture were in the following order: untextured (2.60 – 32.41 g/m), rectangular texture (15.74 – 31.83 g/m), circular texture (8.33 – 27.47 g/m) and triangular texture (12.64 – 24.31 g/m). This represents a 2 % (rectangular texture), 15 % (circular texture) and 25 % (triangular texture) reduction of wear rate due to texturing, implying that the highest wear resistance was obtained with the triangular texture. This is consistent with the findings of other researchers [35,36].

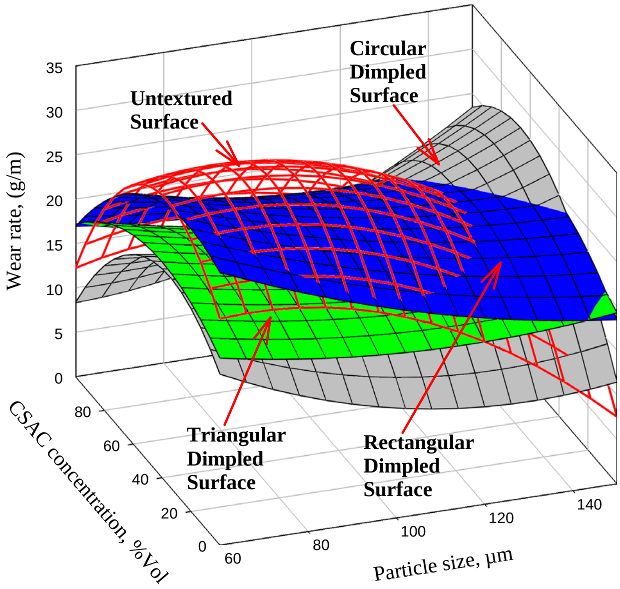

Figure 8. Wear rate variation obtained by the BBD for untextured and circular, rectangular and triangular textured surfaces

The wear rates are different because of the surface textures that influence stresses and hence the interfacial deformations. When friction reached steady-state values, the stress created due to the different texture geometries reduced the interfacial deformation at the contacts, thereby reducing the wear rate, with the triangular texture presenting a decreased maximum wear rate compared with the untextured surface. The wear mechanism changes from abrasion, at the onset of friction to adhesion, at the attainment of steady-state friction. The initial wear particles, produced by abrasion, fill the hollows created by texturing and increase the real contact area.

3.6 Coefficient of friction

It was noticed from Figure 9 that textured samples showed higher predicted values of coefficient of friction than untextured samples, with values in the following order: untextured (0.04 – 0.20), rectangular texture (0.02 – 0.25), triangular texture (0.13 – 0.30) and circular texture (0.10 – 0.45). The minimum coefficient of friction values were in the following order: triangular dimples (0.13), circular dimples (0.10), untextured surface (0.04) and rectangular dimples (0.02).

The low values of the coefficient of friction were due to the nature of the reinforcement materials. Activated carbon is lubricating in nature and untextured samples are expected to have a lower coefficient of friction values than the samples with textured surfaces. As time progressed, some carbon particles might have adhered to the ball surface. This led to induced carbon-to-carbon contact, thereby reducing friction. Over time, the shear strength of the carbon-to-carbon interface became lower, causing the coefficient of friction to decrease further. These results compare well with similar work reported by Nuruzzaman and Chowdhury [37]. The increase in the maximum coefficient of friction values due to texturing was 18 % for rectangular dimples, 32 % for triangular dimples and 55 % for circular dimples, which is consistent with the research findings of Yu et al. [38]. Hence, the circular texture showed the best friction performance, while the untextured surface showed the worst. Furthermore, the tested composites with textured surfaces can find applications in areas that require friction or gripping enhancement including road-tire contact, adhesion, biomimetics, movement transmission and control.

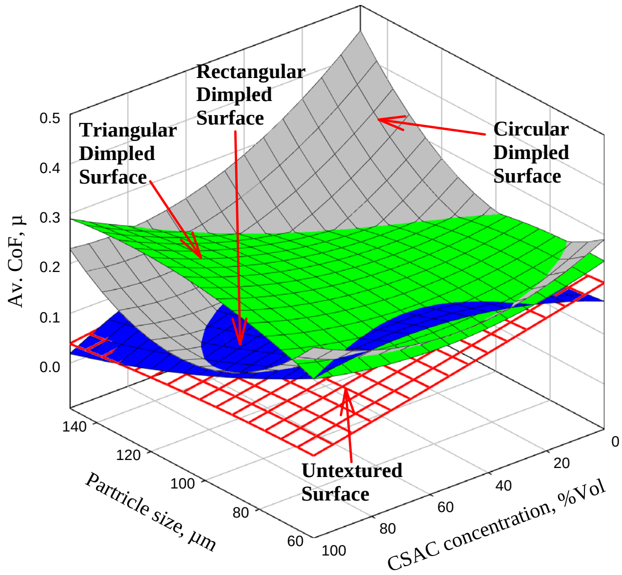

Figure 9. Coefficient of friction (CoF) variation obtained by the BBD for untextured and circular, rectangular and triangular textured surfaces

4. Conclusions

Surface texturing with circular, rectangular and triangular geometries reduced the tribomechanical properties (tensile strength, compressive strength, flexural strength and hardness) of composites while decreasing the wear rate and increasing the coefficient of friction.

The noticed reductions were in the range from 30 % (circular texture) to 67 % (triangular texture) for tensile strength, from 19 % (triangular texture) to 45 % (rectangular texture) for compressive strength and from 23 % (circular texture) to 62 % (triangular texture) for flexural strength. Similarly, hardness reduction was in the range from 12 % (triangular texture) to 14 % (circular texture) and wear rate reduction was in the range from 2 % (rectangular texture) to 25 % (triangular texture). Interestingly, the coefficient of friction increased with texturing showing an increase in the range from 18 % (rectangular texture) to 55 % (circular texture).

Failures of the textured surfaces were due to crack nucleation sites at the dimples periphery. The study has experimentally demonstrated that textured surfaces in dry sliding conditions reduce tyre wear rates while maintaining enough frictional grip.

References

[1] B. Bhushan, Introduction to Tribology, John Wiley & Sons, New York, 2013, DOI: 10.1002/9781118403259

[2] P.P. Gohil, J.M. Mistry, V.P. Chaudhary, Modeling of mechanical properties and morphological analysis of glass fiber nylon 6 composite, in Proceedings of the 2nd International Conference on Civil, Materials and Environmental Sciences (CMES 2015), 13-14.03.2015, London, UK, 196-200, DOI: 10.2991/cmes-15.2015.57

[3] J.R. Ochola, J.I. Mwasiagi, Modelling the influence of cotton fibre properties on ring spun yarn strength using Monte Carlo techniques, Research & Reviews in Polymer, Vol. 3, No. 3, 2012, pp. 84-88.

[4] B. Xu, Y.-l. Ting, Cotton trash measurement using image analysis, in Proceedings of the Beltwide Cotton Conference, 09-12.01.1996, Nashville, USA, pp. 1701-1705.

[5] B. Latha, V.S. Senthilkumar, Modeling and analysis of surface roughness parameters in drilling GFRP composites using fuzzy logic, Materials and Manufacturing Processes, Vol. 25, No. 8, 2010, pp. 817-827, DOI: 10.1080/10426910903447261

[6] L. Hammerström, S. Jacobson, Designed high-friction surfaces – Influence of roughness and deformation of the counter surface, Wear, Vol. 264, No. 9-10, 2008, pp. 807-814, DOI: 10.1016/j.wear.2006.12.082

[7] R. Arvind Singh, L. Siyuan, N. Satyanarayana, T.S. Kustandi, S.K. Sinha, Bio-inspired polymeric patterns with enhanced wear durability for microsystem applications, Materials Science and Engineering C, Vol. 31, No. 7, 2011, pp. 1577-1583, DOI: 10.1016/j.msec.2011.07.006

[8] G. Dumitru, V. Romano, H.P. Weber, H. Haefke, Y. Gerbig, E. Pflüger, Laser microstructuring of steel surfaces for tribological applications, Applied Physics A, Vol. 70, No. 4, 2000, pp. 485-487, DOI: 10.1007/s003390051073

[9] I. Etsion, L. Burstein, A model for mechanical seals with regular microsurface structure, Tribology Transactions, Vol. 39, No. 3, 1996, pp. 677-683, DOI: 10.1080/10402009608983582

[10] I. Etsion, Y. Kligerman, G. Halperin, Analytical and experimental investigation of laser-textured mechanical seal faces, Tribology Transactions, Vol. 42, No. 3, 1999, pp. 511-516, DOI: 10.1080/10402009908982248

[11] J.M. Faulstich de Paiva, A. De Nadai dos Santos, M. Cerqueira Rezende, Mechanical and morphological characterizations of carbon fiber fabric reinforced epoxy composites used in aeronautical field, Materials Research, Vol. 12, No. 3, 2009, pp. 367-374, DOI: 10.1590/S1516-14392009000300019

[12] J.M. Faulstich de Paiva, S. Mayer, M. Cerqueira Rezende, Comparison of tensile strength of different carbon fabric reinforced epoxy composites, Materials Research, Vol. 9, No. 1, 2006, pp. 83-89, DOI: 10.1590/S1516-14392006000100016

[13] Q.B. Guo, M.Z. Rong, G.L. Jia, K.T. Lau, M.Q. Zhang, Sliding wear performance of nano-SiO_2/short carbon fiber/epoxy hybrid composites, Wear, Vol. 266, No. 7-8, 2009, pp. 658-665, DOI: 10.1016/j.wear.2008.08.005

[14] G. Zhang, Structure-tribological property relationship of nanoparticles and short carbon fibers reinforced PEEK hybrid composites, Journal of Polymer Science Part B: Polymer Physics, Vol. 48, No. 7, 2010, pp. 801-811, DOI: 10.1002/polb.21951

[15] G. Zhang, R. Sebastian, T. Burkhart, K. Friedrich, Role of monodispersed nanoparticles on the tribological behavior of conventional epoxy composites filled with carbon fibers and graphite lubricants, Wear, Vol. 292-293, 2012, pp. 176-187, DOI: 10.1016/j.wear.2012.05.012

[16] K. Friedrich, Wear models for multiphase materials and synergistic effects in polymeric hybrid composites, in K. Friedrich (Ed.), Advances in Composite Tribology, Elsevier, Amsterdam, 1993, DOI: 10.1016/B978-0-444-89079-5.50010-6

[17] Z. Zhang, C. Breidt, L. Chang, F. Haupert, K. Friedrich, Enhancement of the wear resistance of epoxy: short carbon fibre, graphite, PTFE and nano-TiO_2, Composites Part A: Applied Science and Manufacturing, Vol. 35, No. 12, 2004, pp. 1385-1392, DOI: 10.1016/j.compositesa.2004.05.005

[18] L. Chang, Z. Zhang, Tribological properties of epoxy nanocomposites: Part II. A combinative effect of short carbon fibre with nano-TiO_2, Wear, Vol. 260, No. 7-8, 2006, pp. 869-878, DOI: 10.1016/j.wear.2005.04.002

[19] B. Cheng, M. Kortschot, A study of the friction coefficients of unidirectional and woven carbon fibre/epoxy composites, Polymers and Polymer

Composites, Vol. 24, No. 4, 2016, pp. 255-263, DOI: 10.1177/096739111602400404

[20] A.A. Ibrahim, Friction and wear of carbon fibres reinforced epoxy composites, Journal of the Egyptian Society of Tribology, Vol. 13, No. 4, 2016, pp. 12-27, DOI: 10.21608/jest.2016.79585

[21] B. Cheng, M. Kortschot, A study of the coefficient of friction and wear of unidirectional and wovencarbon fiber/epoxy composite in severe abrasive conditions, in Proceedings of the 10th International Conference on Composite Science and Technology (ICCST/10), 02-04.09.2015, Lisbon, Portugal, Paper 22.

[22] A. Islam, R. Alam, O. Hannan, Multiresponse optimization based on statistical response surface methodology and desirability function for the production of particleboard, Composites Part B: Engineering, Vol. 43, No. 3, 2012, pp. 861-868, DOI: 10.1016/j.compositesb.2011.11.033

[23] M.A.A. Razali, N. Sanusi, H. Ismail, N. Othman, A. Ariffin, Application of response surface methodology (RSM) for optimization of cassava starch grafted polyDADMAC synthesis for cationic properties, Starch, Vol. 64, No. 12, 2012, pp. 935-943, DOI: 10.1002/star.201200007

[24] R. Govindaraju, S. Jagannathan, M. Chinnasamy, P. Kandhavadivu, Optimization of process parameters for fabrication of wool fiber-reinforced polypropylene composites with respect to mechanical properties, Journal of Engineered Fibers and Fabrics, Vol. 9, No. 3, 2014, pp. 126-133, DOI: 10.1177/155892501400900315

[25] A. Balakrishna, D.N. Rao, A.S. Rakesh, Characterization and modeling of process parameters on tensile strength of short and randomly oriented Borassus Flabellifer (Asian Palmyra) fiber reinforced composite, Composites Part B: Engineering, Vol. 55, 2013, pp. 479-485, DOI: 10.1016/j.compositesb.2013.07.006

[26] S. Panigrahi, X. Li, L. Tabil, Injection moulding processing of flax fibre-reinforced polyethylene biocomposites, in Proceedings of the International Conference on Flax and Other Bast Plants, 21-23.07.2008, Saskatoon, Canada, pp. 399-407.

[27] R. Govindaraju, S. Jagannathan, Optimization of mechanical properties of silk fiber-reinforced polypropylene composite using Box-Behnken experimental design, Journal of Industrial Textiles, Journal of Industrial Textiles, Vol. 47, No. 5, 2016, pp. 602-621, DOI: 10.1177/1528083716667257

[28] A. Athijayamani, R. Ganesamoorthy, K.T. Loganathan, S. Sidhardhan, Modelling and analysis of the mechanical properties of Agave sisalana variegata fibre / vinyl ester composites using Box-Behnken design of response surface methodology, Strojniški vestnik – Journal of Mechanical Engineering, Vol. 62, No. 5, 2016, pp. 273-280, DOI: 10.5545/sv-jme.2015.2641

[29] L.M. Akuwueke, C.V. Ossia, H.U. Nwosu, Optimization of the mechanical properties of chemically activated carbon composites in organic friction linings by Box-Behnken design, Proceedings on Engineering Sciences, Vol. 4, No. 2, 2022, pp. 191-202, DOI: 10.24874/PES04.02.009

[30] C.R. Alavala, Weight loss functions for tolerable wear rate of AA1100/BN metal matrix composites, International Journal of Mechanical Engineering and Technology, Vol. 7, No. 5, 2016, pp. 9-17.

[31] J.-S. Kwak, Application of Taguchi and response surface methodologies for geometric error in surface grinding process, International Journal of Machine Tools and Manufacture, Vol. 45, No. 3, 2005, pp. 327-334, DOI: 10.1016/j.ijmachtools.2004.08.007

[32] M. Manohar, J. Joseph, T. Selvaraj, D. Sivakumar, Application of Box Behnken design to optimize the parameters for turning Inconel 718 using coated carbide tools, International Journal of Scientific & Engineering Research, Vol. 4, No. 4, 2013, pp. 620-642.

[33] A.A. Khemchandani, Kameshwaran, J. Vasanth, Determination of tensile strength of composite laminates with multiple holes, International Journal of Applied Engineering Research, Vol. 14, No. 19, 2019, pp. 3749-3755.

[34] T. Wang, Q. Kang, X. Zhang, X. Xu, W. Li, H. Zhang, Study on the influence of hole defects with different shapes on the mechanical behavior and damage law of coal and rock, PLoS One, Vol. 17, No. 3, 2022, Paper e0265753, DOI: 10.1371/journal.pone.0265753

[35] S. Wos, W. Koszela, P. Pawlus, Comparing tribological effects of various chevron-based surface textures under lubricated unidirectional sliding, Tribology International, Vol. 146, 2020, Paper 106205, DOI: 10.1016/j.triboint.2020.106205

[36] G. Vignesh, D. Barik, S. Aravind, P. Ragupathi, M. Arun, Numerical investigation of dimple-texturing on the turning performance of hardened AISI H-13 steel, International Journal for Simulation and Multidisciplinary Design Optimization, Vol. 13, 2022, Paper 10, DOI: 10.1051/smdo/2021043

[37] D.M. Nuruzzaman, M.A. Chowdhury, Friction and wear of polymer and composites, in N. Hu (Ed.), Composites and Their Properties, IntechOpen, Rijeka, 2012, pp. 301-308, DOI: 10.5772/48246

[38] H. Yu, H. Deng, W. Huang, X. Wang, The effect of dimple shapes on friction of parallel surfaces, Proceedings of the Institution of Mechanical Engineers, Part J: Journal of Engineering Tribology, Vol. 225, No. 8, 2011, pp. 693-703, DOI: 10.1177/1350650111406045